Metallophysics and Advanced Technologies
Металофіз. новітні технол.
Metallofiz. Noveishie Tekhnol.
2026, vol. 48, No. 5, pp. 527–536
https://doi.org/10.15407/mfint.48.05.0527
Reprints available directly from the publisher

PACS numbers: 07.10.Cm, 62.20.de, 62.25.-g, 73.40.Gk, 73.40.Rw, 77.55.+f, 81.70.Bt

Young's Modulus of Sub-10 nm MgO Films *via* the Tunnelling-Current Nanoindenter Method

V. O. Burlakov and O. V. Filatov

G. V. Kurdyumov Institute for Metal Physics, N.A.S. of Ukraine,
36 Academician Vernadsky Blvd.,
UA-03142 Kyiv, Ukraine

A novel method for determining the elastic properties of ultrathin dielectric films based on conductive-tip nanoindentation is applied. The approach enables the extraction of film deformation from variations in tunnelling current, thereby, eliminating contributions from the substrate, indenter, and instrument compliance. A 6 nm MgO film deposited on a Fe film is investigated as a model system. The load–displacement curve is calculated from the obtained data of tunnel current, allowing evaluation of the Young's modulus. The measured modulus of the MgO film is of ≅ 180 GPa, which is lower than bulk values and is attributed to reduced density and structural features of the deposited film. Repeated indentation results in an apparent increase in the Young's modulus up to ≅ 380 GPa, associated with densification and reduced porosity. The applied method provides a high-resolution approach for measuring the mechanical properties of dielectric films with thicknesses below 10 nm.

Key words: nanofilms, Young's modulus, mechanical properties, magnesium oxide MgO, nanoindentation, tunnelling current.

Застосовано новий метод визначення пружніх властивостей надтонких діелектричних плівок на основі наноіндентування провідним вістрям. Цей підхід уможливлює виокремити деформацію плівки за зміною тунельного струму, тим самим усуваючи внески від підкладинки, індентора та

Corresponding author: Viktor Oleksandrovych Burlakov
E-mail: odinpwnzpacan@gmail.com

Citation: V. O. Burlakov and O. V. Filatov, Young's Modulus of Sub-10 nm MgO Films *via* the Tunnelling-Current Nanoindenter Method, *Metallofiz. Noveishie Tekhnol.*, **48**, No. 5: 527–536 (2026). DOI: 10.15407/mfint.48.05.0527

податливости приладу. Плівка MgO товщиною у 6 нм, нанесена на плівку Fe, досліджується як модельна система. Крива навантаження–зміщення розраховується на основі одержаних даних стосовно тунельного струму, що дає змогу оцінити модуль Юнґа. Виміряний модуль плівки MgO становить ≅ 180 ГПа, що нижче за об'ємні значення та може бути пов'язано з пониженням густини та структурними особливостями нанесеної плівки. Повторне індентування приводить до помітного збільшення модуля Юнґа до ≅ 380 ГПа, що пов'язане з ущільненням і пониженням пористости. Застосований метод забезпечує дієвий підхід для міряння механічних властивостей діелектричних плівок товщиною менше 10 нм.

Ключові слова: наноплівки, модуль Юнґа, механічні властивості, оксид Маґнію MgO, наноіндентування, тунельний струм.

(Received 10 April, 2026; in final version, 20 April, 2026)

1. INTRODUCTION

Ultrathin dielectric films and multilayers with thicknesses below 10 nm are central to nanoelectronic, spintronic, and quantum technologies [1, 2]. Continued miniaturization of high-frequency devices and next-generation CMOS systems requires dielectric layers only a few atomic layers thick to achieve high capacitance and low power consumption [3]. In such architectures, mechanical integrity is critical, as the films must withstand stresses induced by thermal expansion mismatch and applied electric fields without fracture or delamination [4, 5].

Beyond their electronic functionality, ultrathin films are also crucial for nanoelectromechanical systems (NEMS), where elastic deformation and dynamic response are determined by mechanical properties. Device miniaturization enhances sensitivity, enabling sub-femtometer-displacement resolution and zepto-scale mass and force detection [6–9].

Consequently, understanding the thickness dependence of elastic properties at the nanoscale is of fundamental and technological importance. At these scales, surface and dopant effects become dominant, leading to mechanical properties that can deviate significantly from bulk properties, exhibiting either softening or stiffening [10]. Thickness-dependent elasticity primarily arises from the high proportion of surface atoms, which may decrease stiffness since surface atoms have less restrictions on their movement [11] or increase it through electron charging redistribution and bond contraction [12, 13]. These effects have been both analysed (using continuum and atomistic approaches [13–16]) and confirmed experimentally [16, 17].

Within the field of green electronics called spintronics, in which magnetic tunnel junctions incorporating an MgO barrier layer serve as key components in magnetic memory devices, magnetic sensors, radio-frequency and microwave applications, as well as logic and non-Boolean devices [18–20]. MgO seems to be one of the best candidates for use as a barrier layer due to its high dielectric constant and wide band gap. In addition, its cubic crystal structure ensures a relatively low lattice mismatch with many metals and semiconductors [21]. MgO thin films used as barrier layers enable high tunnelling magnetoresistance ratios *via* coherent spin-polarized tunnelling [22]. Therefore, MgO is selected as a model system for the present study, since the determination of its Young's modulus is essential for evaluating the mechanical stability and reliability of ultrathin barrier layers in nanoscale electronic and spintronic devices.

2. EXPERIMENTAL DETAILS

Accurate determination of the elastic properties of ultrathin films remains experimentally challenging, as most conventional techniques lack sufficient sensitivity for thicknesses below 10 nm [23, 24]. Commonly employed methods, such as nanoindentation, typically provide reliable characterization for films with thicknesses on the order of several hundred nanometres, particularly when combined with advanced modelling [25, 26].

To solve this problem, a novel approach to determining the mechanical properties of ultrathin dielectric films is presented. In this method, a conductive tip replaces the traditional diamond tip. The dielectric film under investigation is deposited onto a conductive substrate, and a constant potential difference is applied between the tip and the substrate (Fig. 1).

The current flowing through the tip–dielectric–substrate system is continuously monitored during the indentation process. Variations in the tunnel current result from changes in the dielectric film's thickness and defect mobility under applied load. By analysing these changes, a load–displacement curve is calculated, providing insights into the mechanical behaviour of the dielectric film.

The indenter is fabricated from hardened steel and is characterized by a truncated conical geometry with a tip area of $A \cong 4.8 \cdot 10^{-9}$ m^2. Prior to the measurements, the applied load is calibrated using standard reference weights. The corresponding calibration data are obtained by several measurements.

The dielectric film is a 6 nm thick MgO layer deposited under vacuum conditions onto a 100 nm thick Fe film. The tunnelling current between the tip and the underlying Fe film is measured using the electrical circuit shown in Fig. 1. A Zener diode is employed to maintain a constant bias voltage of 0.7 V. The tunnelling current is determined from the voltage drop across the reference resistor, allowing for quan-

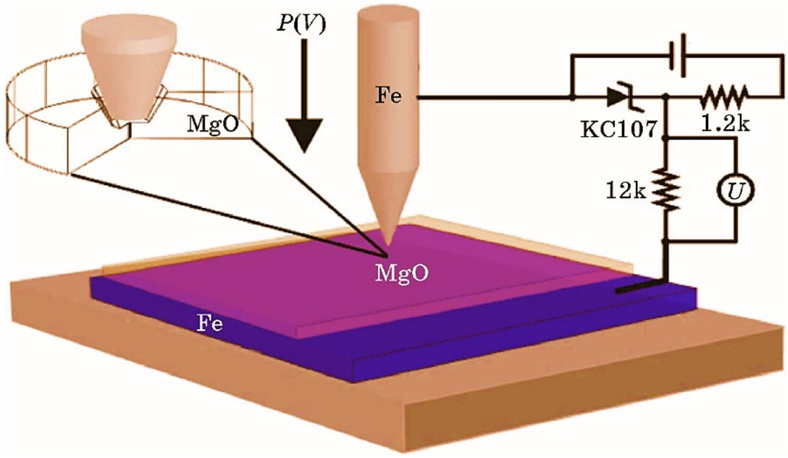

Fig. 1. Schematic representation of the tunnelling current nanoindenter method: a constant bias voltage is applied between the conductive indenter and the substrate, while the tunnelling current through the tip–dielectric–substrate system is monitored during loading to determine the deformation of the dielectric film.

titative analysis during indentation. The change in dielectric thickness under applied load from the tip is inferred from the corresponding variation in the tunnelling current.

3. RESULTS AND DISCUSSION

Reduced atomic co-ordination near a free surface leads to charge redistribution and changes in bonding, resulting in elastic properties that differ from those of the bulk material. While the surface region is only a few atomic layers thick and can be neglected in micron-scale structures, its influence becomes significant at the nanoscale because of the increased surface-to-volume ratio. As a result, the overall stiffness of a nanoscale film cannot be accurately described using the bulk modulus. In this context, the concept of an effective modulus is used to characterize the averaged mechanical response of a structurally inhomogeneous system. Nanoscale films must be regarded as inhomogeneous, since surface regions contribute substantially to their elastic behaviour. Consequently, the effective modulus becomes size-dependent and deviates from the corresponding bulk value [27, 28].

The Young's modulus determined by indentation is typically evaluated using the load–displacement (P–h) curve [29]. The indenter displacement under loading is influenced by the deformation of the film, the substrate, the indenter, and the instrument itself. This complicates the isolation of the film deformation contribution to the total displacement h. When a conductive indenter is employed, the displacement (h_f) associated with the deformation of the dielectric film is determined from variations in the tunnelling current. At room temperature, the tunnelling current exhibits an approximately exponential dependence on the applied voltage. At low voltages (up to $\cong 0.3$ V) [30], thermal fluctuations significantly affect the current, introducing a source of error in the exponential approximation of the current–voltage relationship.

The exponential dependence of the tunnelling resistance provides high resolution in determining variations in the dielectric thickness. Under loading with a conductive indenter tip, the electrical resistance of the system is observed to vary in the range from 10 MΩ to 1 kΩ as the dielectric thickness decreases from 5 nm to 1 nm. The contact resistance between the indenter tip and the metallic film, without the dielectric film, is approximately 100 Ω and decreases linearly with increasing contact area. Its influence on the total tunnelling current is therefore negligible. Consequently, the displacement (h_f) calculated from variations in the tunnelling current I enables the determination of the dielectric deformation, while excluding contributions from the deformation of the substrate, the indenter, and the instrument.

During the experiment, the voltage across a reference resistor connected in series with the sample is monitored. Variations in the dielectric thickness affect both the current I in the circuit and the voltage U_f across the sample (Fig. 2). In Ref. [31], a series of I–U characteristics

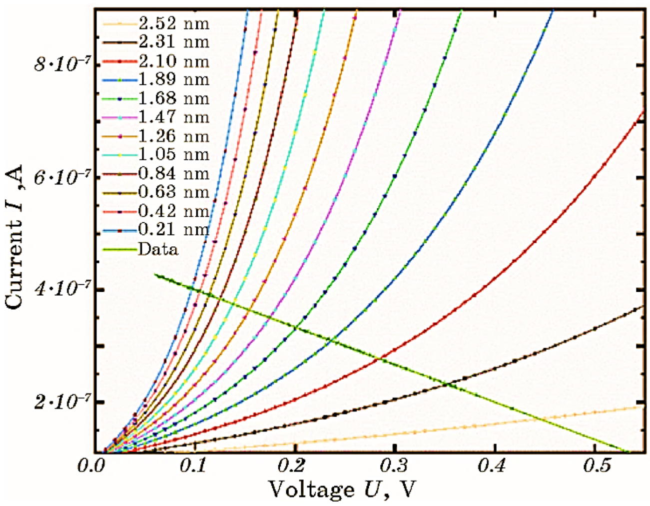

Fig. 2. Determination of dielectric thickness: the I–U_f characteristic (data line) measured during deformation is matched with calculated I–U curves for different MgO thicknesses (2.52–0.21 nm lines).

for different MgO thicknesses is experimentally obtained, and an empirical relationship for their calculation over a wide range of dielectric thicknesses is proposed. This relationship is used to determine the dielectric thicknesses by matching the measured I–U_f characteristic with the calculated I–U characteristics (Fig. 2).

The I–U_f characteristics obtained during the deformation of MgO intersects the calculated I–U characteristics corresponding to different dielectric thicknesses with a step of 0.21 nm. Using the intersection points, the values of the exp(h_f) on current I is constructed (Fig. 3). This relationship is approximated by a linear function in the selected co-ordinates. The dielectric deformation is then determined from the obtained functional relationship $h_f = f(\ln(I))$.

Based on the obtained data, the load–displacement curve ($P = f(h_f)$) is constructed (Fig. 4).

The loading is performed within the elastic deformation regime of the dielectric film (up to 10 MPa). No residual imprints associated with plastic deformation are observed during microscopic examination of the film surface, and the unloading curve returns to the initial point. The resulting diagram corresponds to the load–displacement response characteristic of instrumented (kinetic) indentation. The Young's modulus of the film is determined from the slope of the unloading curve in the range of $(0.8–0.4)P_{max}$. This portion of the curve is approximated by a linear function: red dash line in Fig. 4.

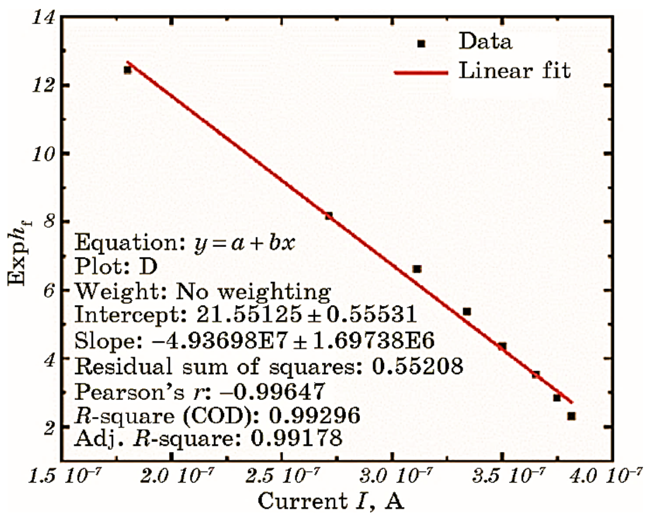

Fig. 3. Determination of dielectric deformation: the values of exp(h_f) on tunnelling current I constructed from the intersection points of experimental I–U_f characteristic and calculated I–U curves. The solid line is a linear fit in the selected co-ordinates.

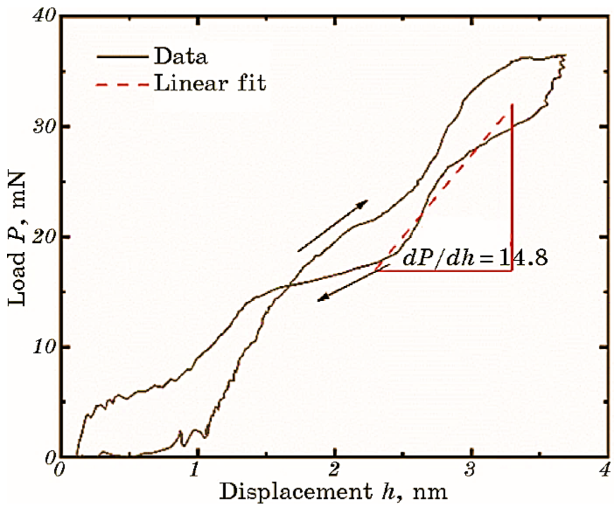

Fig. 4. Load–displacement curve of the MgO film obtained from tunnelling-current measurements.

Conventionally [29], the evaluation of the Young's modulus in indentation is performed using equations that account for the deformation of the indenter and the compliance of the measuring system. In the present study, the calculation is simplified, since only the deformation of the film is considered in constructing the load–displacement curve. Using the value of the Poisson's ratio of the MgO film [32], the contact area, and the slope of the unloading curve, the Young's modulus is calculated as:

$$E = \frac{\sqrt{\pi}(1-\nu^2)}{2\sqrt{A}}\frac{dP}{dh}, \qquad (1)$$

where E is the Young's modulus, ν is the Poisson's ratio, A is the tip area.

The Young's modulus obtained for a 5 nm thick MgO film deposited on a 100 nm thick Fe film is $\cong$ 180 GPa. For bulk MgO, the Young's modulus ranges from 250 to 350 GPa depending on the crystallographic orientation [33]. The density of polycrystalline MgO is known to affect significantly the Young's modulus, which may vary within the range of 80–300 GPa [34]. Based on these data, the MgO film deposited by vacuum sputtering is estimated to have a density of approximately 3.2 g/cm^3, which is about 10% lower than that of single-crystalline MgO.

During repeated indentation at the same point, the load–displacement curve is determined using the same procedure. The resulting curve exhibits reduced hysteresis between the loading and un-

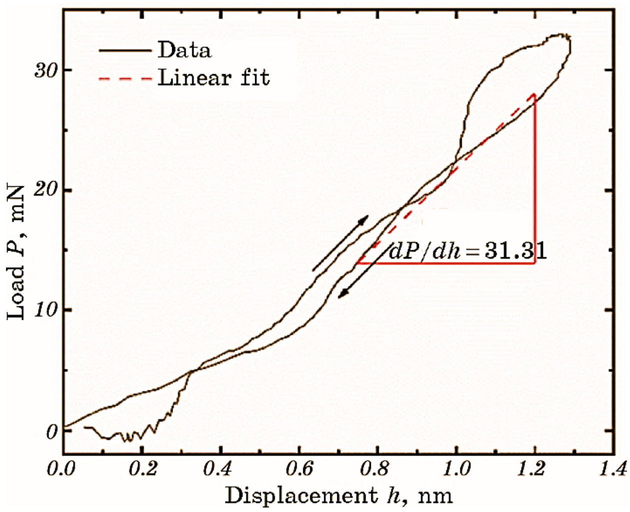

Fig. 5. Load–displacement curve obtained during repeated indentation at the same location of the MgO film.

loading curves, as well as smaller displacement under the same applied load (Fig. 5). The Young's modulus of the MgO film obtained under repeated loading is ≅ 380 GPa, which exceeds the reported values for bulk MgO [34]. The observed twofold increase in the Young's modulus can be attributed to the absence of plastic deformation and a reduction in porosity during repeated indentation.

4. CONCLUSION

A conductive-tip indentation method based on tunnelling current measurements is used to determine the elastic properties of ultrathin dielectric films. The proposed approach enables direct determination of dielectric film deformation by isolating its contribution from the total displacement, overcoming limitations of conventional nanoindentation techniques at the nanoscale.

Application of the method to MgO films with thicknesses below 10 nm demonstrates its capability to thickness changes and to calculating reliable load–displacement curves. The obtained Young's modulus of ≅ 180 GPa is consistent with bulk values of MgO with reduced density.

Repeated loading leads to a significant increase in the measured modulus to ≅ 380 GPa, which is associated with structural densification and a decrease in porosity. These results indicate that the mechanical properties of ultrathin films are strongly influenced by their structural state and loading history.

This contribution was created under the support of the project of the N.A.S. of Ukraine (No. 0122U002366).

AUTHORS' CONTRIBUTIONS

V. O. Burlakov performed the literature review and analysis of the current state of research, prepared the samples, and carried out the experimental investigations. Data acquisition, processing, and interpretation were conducted by V. O. Burlakov, including the implementation of the proposed method and the calculation of the mechanical properties of the investigated films.

O. V. Filatov supervised the overall direction of the research and provided methodological guidance. O. V. Filatov contributed to the development of the experimental approach, created software for processing the results, participated in the analysis and verification of the obtained results, and assisted in the interpretation of the data and theoretical considerations.

The manuscript, including the main text, discussion, and conclusions, was prepared jointly by both authors. All authors reviewed, revised, and approved the final version of the paper.

REFERENCES

1. T. D. Frazer, J. L. Knobloch, J. N. Hernández-Charpak, K. M. Hoogeboom-Pot, D. Nardi, S. Yazdi, W. Chao, E. H. Anderson, M. K. Tripp, S. W. King, H. C. Kapteyn, M. M. Murnane, and B. Abad, *Phys. Rev. Mater.*, **4**: 073603 (2020).
2. M. Bibes, J. E. Villegas, and A. Barthélémy, *Adv. Phys.*, **60**, Iss. 1: 5 (2011).
3. H. H. Radamson, X. He, Q. Zhang, J. Liu, H. Cui, J. Xiang, Z. Kong, W. Xiong, J. Li, J. Gao, H. Yang, S. Gu, X. Zhao, Y. Du, J. Yu, and G. Wang, *Micromachines*, **10**, Iss. 5: 293 (2019).
4. J.-H. Kim, H.-J. Kil, S. Lee, J. Park, and J.-W. Park, *ACS Omega*, **7**, Iss. 29: 25219 (2022).
5. Z. Zhao, H. Fu, R. Tang, B. Zhang, Y. Chen, and J. Jiang, *Int. J. Smart Nano Mater.*, **14**, Iss. 4: 510 (2023).
6. J. Moser, J. Güttinger, A. Eichler, M. J. Esplandiu, D. E. Liu, M. I. Dykman, and A. Bachtold, *Nature Nanotechnol.*, **8**: 493 (2013).
7. Y. T. Yang, C. Callegari, X. L. Feng, K. L. Ekinci, and M. L. Roukes, *Nano Lett.*, **6**, Iss. 4: 583 (2006).
8. M. Li, H. X. Tang, and M. L. Roukes, *Nature Nanotechnol.*, **2**: 114 (2007).
9. P. X.-L. Feng, *2020 IEEE 33rd Int. Conf. Micro Electro Mech. Syst. (MEMS)*, p. 212 (2020).
10. L. G. Zhou and H. Huang, *Appl. Phys. Lett.*, **84**: 1940 (2004).
11. R. J. Wang, C. Y. Wang, and Y. T. Feng, *Int. J. Mech. Sci.*, **130**: 267 (2017).
12. C. Cheng, P. S. Grant, and L. Lührs, *Adv. Electron. Mater.*, **6**, Iss. 1: 1900364 (2020).

13. C. Q. Sun, *Prog. Solid State Chem.*, **35**, Iss. 1: 1 (2007).
14. W. Xia and S. Keten, *J. Mater. Res.*, **30**: 36 (2015).
15. B. Gong, Q. Chen, and D. Wang, *Mater. Lett.*, **67**: 165 (2012).
16. Z. Ao and S. Li, *Nanoscale Res. Lett.*, **6**: 243 (2011).
17. K. Meganathan, G. Mangamma, M. J. Swaminadhan, V. Murugan, N. B. Shinde, S. Ghosh, and S. K. Eswaran, *J. Phys. Chem. Lett.*, **15**, Iss. 15: 4206 (2024).
18. B. Dieny, I. L. Prejbeanu, K. Garello, P. Gambardella, P. Freitas, R. Lehndorff, W. Raberg, U. Ebels, S. O. Demokritov, J. Akerman, A. Deac, P. Pirro, C. Adelmann, A. Anane, A. V. Chumak, A. Hirohata, S. Mangin, M. C. Onbaşlı, M. d'Aquino, G. Prenat, G. Finocchio, L. Lopez Diaz, R. Chantrell, O. Chubykalo-Fesenko, and P. Bortolotti, *Nature Electron.*, **3**: 446 (2020).
19. V. Burlakov, O. Filatov, and O. Pogorelov, *phys. status solidi (b)*, **258**, Iss. 4: 2000502 (2021).
20. V. O. Burlakov, O. E. Pogorelov, and O. V. Filatov, *Metallofiz. Noveishie Tekhnol.*, **42**, No. 7: 919 (2020) (in Ukrainian).
21. R. Lewandkyw, M. Grodzicki, P. Mazur, and A. Ciszewski, *Acta Phys. Pol. A*, **141**, No. 2: 116 (2022).
22. L. M. Kandpal, B. Taudul, E. Monteblanco, A. Kumar, K. Katcko, F. Schleicher, P. Gupta, S. Boukari, W. Weber, V. Da Costa, J. D. Costa, T. Böhnert, R. Ferreira, P. Freitas, M. Hehn, M. Alouani, P. K. Muduli, D. Lacour, and M. Bowen, *npj Spintronics*, **3**: 2 (2025).
23. V. O. Burlakov and O. V. Filatov, *Progress in Physics of Metals*, **26**, No. 4: 968 (2025).
24. J. N. Hernandez-Charpak, K. M. Hoogeboom-Pot, Q. Li, T. D. Frazer, J. L. Knobloch, M. Tripp, S. W. King, E. H. Anderson, W. Chao, M. M. Murnane, H. C. Kapteyn, and D. Nardi, *Nano Lett.*, **17**, Iss. 4: 2178 (2017).
25. K. Geng, F. Yang, and E. A. Grulke, *Mater. Sci. Eng. A*, **479**, Iss. 1–2: 157 (2008).
26. J. Hay and B. Crawford, *J. Mater. Res.*, **26**: 727 (2011).
27. R. Dingreville, J. Qu, and M. Cherkaoui, *J. Mech. Phys. Solids*, **53**, Iss. 8: 1827 (2005).
28. A. I. Fedorchenko, A. B. Wang, and H. H. Cheng, *Appl. Phys. Lett.*, **94**: 151904 (2009).
29. W. C. Oliver and G. M. Pharr, *J. Mater. Res.*, **7**: 1564 (1992).
30. J. G. Simmons, *J. Appl. Phys.*, **34**, Iss. 6: 1793 (1963).
31. V. O. Burlakov, O. Ye. Pohorelov, and O. V. Filatov, *Metallofiz. Noveishie Tekhnol.*, **45**, No. 2: 157 (2023).
32. *II–VI and I–VII Compounds; Semimagnetic Compounds* (Eds. O. Madelung, U. Rössler, and M. Schulz) (Berlin: Springer: 1999).
33. J. J. Swica and W. B. Crandall, *J. Am. Ceram. Soc.*, **48**, Iss. 2: 102 (1965).
34. D. Chung, J. J. Swica, and W. B. Crandall, *J. Am. Ceram. Soc.*, **46**, Iss. 9: 452 (1963).